Mixed Linear (M,Sb) Chains in the New Antimonides $Hf_{10}M_{\delta}Sb_{6-\delta}$ (M = V, Cr, Mn, Fe, Co, Ni, Cu): Crystal and Electronic Structures, Phase Ranges, and Electrical and Magnetic Properties

Holger Kleinke,*[a,b] Christel Ruckert,[b] and Claudia Felser[c]

Keywords: Metal-rich antimonides / Magnetism / Structure and bonding / Conductivity / LMTO

The title compounds can be synthesized in quantitative yields by arc-melting of stoichiometric amounts of $HfSb_2$, Hf and one of the *3d* metals V, Cr, Mn, Fe, Co, Ni, and Cu. These antimonides crystallize in a substitution variant of the W_5Si_3 type, in which one position is statistically mixed, occupied by the *3d* metal atom M or the Sb2 atom in different ratios. Within the linear (M,Sb) chain, the M:Sb ratio may vary between 3:1 and 2:3. According to calculations of the electronic structures of $Hf_{10}M_{\delta}Sb_{6-\delta}$ with $\delta = 1$, these phases are metallic compounds stabilized by strong Hf–Hf, Hf–M, and Hf–Sb bonds, and to a smaller extent by bonding interactions within the linear (M,Sb) chain. The metallic character was confirmed by measurements of the electrical resistivity and the magnetism of selected samples. Whereas Pauli paramagnetism was observed experimentally for M = V, Co, and Ni, $Hf_{10}FeSb_5$ is apparently the only phase with localized magnetic moments and magnetic coupling. This is in agreement with the magnetic ground state obtained solely for the ordered structure model of $Hf_{10}FeSb_5$ with spin-polarized calculation within the local spin density approximation.

Introduction

The W_5Si_3 type is adopted by a variety of different phases, including mainly silicides, germanides and stannides of the valence electron-poor (so-called "early") transition metal atoms T.[1] In this structure type, linear chains of the T atoms run parallel to linear chains of main group elements E along [001] with the same interatomic distances in both chains. As a consequence a matrix effect, i.e. somewhat short T−T and long E−E distances or vice versa, may occur.

It is assumed that the W_5Si_3 structure type is basically limited to compounds of the third and fourth main group because the pnicogen and chalcogen atoms Q will most likely not form short Q−Q bonds in such metal-rich phases. Exceptions are the tellurides $M_xK_4Te_3$ (M = Ca, Sr)[2] which can be considered as electron-precise compounds $(M^{+2})_{0.5}(K^{+1})_4(Te^{-1})(Te^{-2})_2$, each Te^{-1} forming two one-electron-two-center bonds. However, one binary vanadium arsenide was described to crystallize in the W_5Si_3 structure type, the structure of which exhibits either a disordered As or a mixed (V,As) chain, thus reducing the As−As interactions.[3] Three examples based on antimony ($Zr_5M_{\delta}Sb_{3-\delta}$, M = Fe, Co, Ni, $\delta \approx 0.5$) are already known and show an incorporation of ca. 50% M atoms in the linear antimony chain.[4] Although alternating the M and Sb atoms within this chain would maximize the M−Sb bonds and prohibit the occurrence of Sb−Sb bonds, no long-range ordering was observed. This is probably a consequence of the gain in the configurational entropy. Note that each individual chain might be ordered, but in that case there could be no ordering between the chains, i.e. within the *a,b* plane.

In this paper, we present the results of our investigations of the Hf−M−Sb system with the *3d* metal atoms from titanium to copper. This includes different methods for the synthesis of the compounds $Hf_{10}M_{\delta}Sb_{6-\delta}$ (M = V, Cr, Mn, Fe, Co, Ni, and Cu), their crystal and electronic structures, phase ranges and magnetic properties. The phases $Hf_{10}M_{\delta}Sb_{6-\delta}$ are isostructural with the corresponding zirconium antimonides, which is not an obvious result, as investigations of ternary zirconium hafnium phosphides showed.[5−6]

Results and Discussion

Crystal Structure

The hitherto unknown antimonides $Hf_{10}M_{\delta}Sb_{6-\delta}$ (M = V, Cr, Fe, Mn, Co, Ni, Cu) occur in ternary variants of the W_5Si_3 structure type, the Hf atoms occupying the W sites and the M and Sb atoms replacing the Si atoms (Figure 1). Whereas the *8h* position is filled solely by antimony (Sb1), the *4a* site is occupied by mixtures of the M and Sb2 atoms without long-range ordering.

This comes along with a linear (M,Sb) chain with interatomic distances of approximately 280 pm which is surrounded by eight Hf2 atoms that form chains of face-condensed distorted square antiprisms (right part of Figure 2). The chains of Hf antiprisms, sheathed by the Sb2 atoms, are interconnected by Hf2−Hf2 bonds of ca. 320 pm to a

[a] Department of Chemistry, University of Waterloo, Waterloo, Ontario, Canada N2L 3G1
Fax: (internat.) + 1-519/746-435
E-mail: Kleinke@sciborg.uwaterloo.ca
[b] FB Chemie und Wissenschaftliches Zentrum für Materialwissenschaften der Philipps-Universität, Hans-Meerwein-Straße, D-35032 Marburg, Germany
[c] Institut für Anorganische Chemie und Analytische Chemie der J.-Gutenberg-Universität, Duesbergweg 10−14, D-55099 Mainz, Germany

  1434−1948/00/0202−315 $ 17.50+.50/0

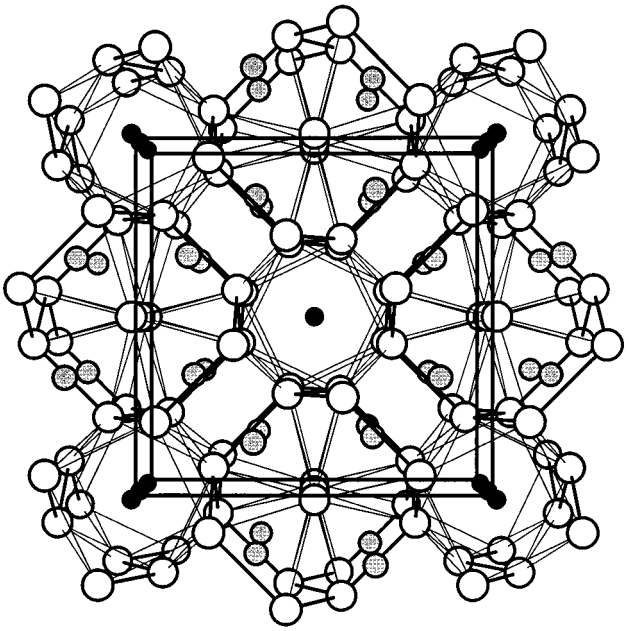

Figure 1. Structure of $Hf_{10}M_{\delta}Sb_{6-\delta}$ in a projection along the *c* axis; large, white circles: Hf; medium, gray: Sb; small, black: (M,Sb); Hf−Hf distances < 340 pm are indicated by bold lines

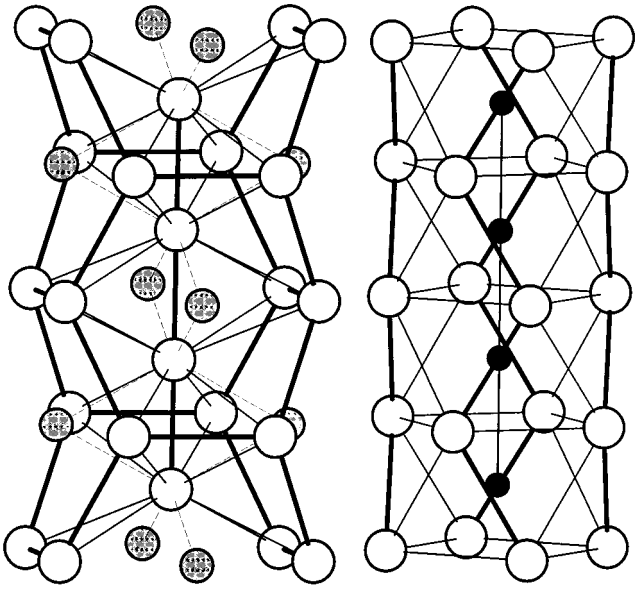

Figure 2. Columnar structure motifs of $Hf_{10}M_{\delta}Sb_{6-\delta}$; left: Chain of Hf1, surrounded by 8 Hf2 and 4 Sb1 atoms; the $Hf1Sb_4$ tetrahedra are indicated by dashed lines; right: chain of (M,Sb), situated in face-sharing $Hf2_8$ square antiprisms; Hf−Hf distances < 340 pm are indicated by bold lines

three-dimensional network surrounding linear chains of the Hf1 atoms ($d_{Hf1-Hf1} \approx 280$ pm). The Hf1 atoms are located in Sb_4 tetrahedra (left part of Figure 2), which are condensed via common vertices to form linear chains parallel to [001].

One can therefore divide the Hf−Hf distances into three classes. The first one includes the bonds within the linear Hf1 chain (ranging from $d = 277$ pm in $Hf_{10}Fe_{1.54}Sb_{4.46}$ to $d = 280$ pm in $Hf_{10}V_{0.80}Sb_{5.20}$ and $Hf_{10}V_{0.88}Sb_{5.12}$). The second one includes the distances of ca. 320−330 pm, and the third the longer ones of ca. 350 pm. These may be compared to elemental hafnium in its hexagonal modification with Hf−Hf distances of 313 and 320 pm, or to another Hf-rich antimonide, Hf_6NiSb_2, the structure of which exhibits Hf−Hf distances between 321 and 329 pm.[7] These comparisons reveal the extraordinary shortness of the bonds of class 1.

The Hf−Sb1 distances vary from 288 to 292 pm depending on the metal atom M and the δ parameter. The Hf−Sb2 bond lengths are somewhat shorter (between 278 and 289 pm); they are equal to the Hf−M distances by symmetry, which results in averaged values: since all M atoms are smaller than an Sb atom (e.g. the Pauling single bond radii: $r_V = 122$ pm, $r_{Ni} = 115$ pm, $r_{Cu} = 118$ pm, $r_{Sb} = 139$ pm[8]), the Hf−M distances are longer and the Hf−Sb2 distances shorter than in analogous compounds. This correlates well with the increase of the Hf2−(M,Sb2) distances with decreasing δ (Table 1), which range from 278 pm (δ = 1.54, M = Fe) to 289 pm (δ = 0.80 and 0.88, M = V). Correspondingly, the Hf−Sb distances of 296−297 pm in the structure of Hf_6NiSb_2 are much longer than the Hf−Ni bonds in the same structure (259 pm).[7]

The short Hf2−(M,Sb2) distance in the structure of $Hf_{10}Fe_{1.5}Sb_{4.5}$, i.e. in the case of the highest δ parameter (1.5), is reflected in a significant shift of the Hf2 atom towards the (M,Sb2) chain relative to all other examples with $0.80 \leq \delta \leq 1.18$ (see Table 2). This shift occurs with significantly smaller Hf2−Hf2 distances within the square antiprisms, but larger ones between the prisms (i.e. 334 pm vs. 320−321 pm) and between Hf1 and Hf2 (354 pm vs. 349−350 pm).

Electronic Structure

We successfully synthesized $Hf_{10}MSb_5$ with a variety of *3d* M atoms ranging from vanadium to copper. For a qualitative discussion of the influence of M on the electronic structure and thereby on the physical properties, the electronic structures were calculated for M = V and M = Ni, which are the most *d*-electron-poor and -rich examples, respectively (except for Cu). To model different possibilities of the ordering in the (M,Sb) chain, we calculated three hypothetical structures twice using the Extended Hückel approximation, i.e. in the Hf−V−Sb and in the Hf−Ni−Sb system. In model **I**, an ordering corresponding to the symmetry of space group *I*422 is assumed. In this case, M and Sb alternate in the two chains of the body-centered unit cell, with M of one chain being situated at the Sb position of the other chain, and thus exhibits the same *z* parameter. In model **II**, M and Sb also alternate within each chain, but the M atoms are located at the same positions in both chains of the body-centered unit cell. In model **III**, one chain consists only of M atoms and the other solely of Sb atoms. Models **II** and **III** can be described in the space groups *P*4/*nbm* and *P*4/*mcc*, respectively. In all cases, the stoichiometry remains the same, namely $Hf_{10}MSb_5$.

Table 1. Interatomic distances [pm] of $Hf_{10}M_{\delta}Sb_{6-\delta}$

	mult.	$Hf_{10}V_{0.80}Sb_{5.20}$	$Hf_{10}V_{0.88}Sb_{5.12}$	$Hf_{10}Mn_{1.16}Sb_{4.84}$	$Hf_{10}Fe_{1.54}Sb_{4.46}$	$Hf_{10}Ni_{1.18}Sb_{4.82}$
Hf1−Hf1	2 ×	279.08(5)	280.20(5)	277.6(1)	277.00(5)	279.45(5)
Hf1−Sb1	4 ×	289.7(1)	289.95(9)	289.5(3)	287.8(1)	289.7(1)
Hf1−Hf2	8 ×	350.00(9)	350.45(8)	349.2(2)	354.27(9)	350.36(9)
Hf2−X	2 ×	288.66(8)	288.72(7)	287.3(2)	277.50(8)	288.53(8)
Hf2−Sb1	1 ×	291.8(1)	291.7(1)	290.2(4)	288.8(2)	291.7(2)
Hf2−Sb1	1 ×	293.4(1)	293.5(1)	293.0(4)	292.7(1)	293.6(1)
Hf2−Hf2	1 ×	320.6(1)	320.9(1)	320.3(3)	334.1(1)	320.9(1)
Hf2−Sb1	2 ×	322.75(8)	323.81(7)	321.3(2)	324.67(9)	323.17(8)
Hf2−Hf2	2 ×	325.02(7)	326.00(7)	323.5(2)	319.78(7)	325.42(7)
Hf2−Hf1	2 ×	350.00(9)	350.45(8)	349.2(2)	354.27(1)	350.36(9)
Hf2−Hf2	2 ×	355.12(8)	355.75(7)	353.2(2)	346.27(8)	355.07(8)
Hf2−Hf2	2 ×	357.4(1)	357.0(1)	355.8(3)	340.1(1)	357.0(1)
Sb1−Hf1	2 ×	289.7(1)	289.95(9)	289.5(3)	287.8(1)	289.7(1)
Sb1−Hf2	2 ×	291.8(1)	291.7(1)	290.2(4)	288.8(2)	291.7(2)
Sb1−Hf2	2 ×	293.4(1)	293.5(1)	293.0(4)	292.7(1)	293.6(1)
Sb1−Hf2	4 ×	322.75(8)	323.81(7)	321.3(2)	324.67(9)	323.17(8)
Sb1−Sb1	2 ×	387.0(1)	387.8(1)	384.1(3)	382.2(1)	387.3(1)
X−X	2 ×	279.08(5)	280.20(5)	277.6(1)	277.00(5)	279.45(5)
X−Hf2	8 ×	288.66(8)	288.72(7)	287.3(2)	277.50(8)	288.53(8)

X = (M/Sb2) position.

Table 2. Atomic positions, equivalent displacement parameters and occupancy factors for $Hf_{10}M_{\delta}Sb_{6-\delta}$

Atom	site	*x*	*y*	*z*	$U_{eq}/(10^4 pm^2)$	occupancy
Hf1	*4b*	0	1/2	1/4	0.0105(3)	100%
Hf2	*16k*	0.07592(7)	0.21745(7)	1/2	0.0108(2)	100%
Sb1	*8h*	0.1636(1)	0.3364(1)	0	0.0091(3)	100%
V/Sb2	*4a*	0	0	1/4	0.013(1)	40(2)% V, 60% Sb
Hf1	*4b*	0	1/2	1/4	0.0058(3)	100%
Hf2	*16k*	0.07594(6)	0.21722(6)	1/2	0.0062(2)	100%
Sb1	*8h*	0.16362(9)	0.33638(9)	0	0.0044(3)	100%
V/Sb2	*4a*	0	0	1/4	0.0065(9)	44(2)% V, 56% Sb
Hf1	*4b*	0	1/2	1/4	0.0141(8)	100%
Hf2	*16k*	0.0759(2)	0.2171(2)	1/2	0.0113(5)	100%
Sb1	*8h*	0.1642(3)	0.3358(3)	0	0.0093(8)	100%
Mn/Sb2	*4a*	0	0	1/4	0.008(3)	58(5)% Mn, 42% Sb
Hf1	*4b*	0	1/2	1/4	0.0129(4)	100%
Hf2	*16k*	0.07357(7)	0.20887(8)	1/2	0.0105(2)	100%
Sb1	*8h*	0.1643(1)	0.3358(1)	0	0.0079(4)	100%
Fe/Sb2	*4a*	0	0	1/4	0.009(1)	77(3)% Fe, 23 Sb
Hf1	*4b*	0	1/2	1/4	0.0064(4)	100%
Hf2	*16k*	0.07600(7)	0.21718(7)	1/2	0.0072(3)	100%
Sb1	*8h*	0.1636(1)	0.3364(1)	0	0.0054(4)	100%
Ni/Sb2	*4a*	0	0	1/4	0.007(1)	59(3)% Ni, 41% Sb

For general considerations, we will discuss model **I** of $Hf_{10}MSb_5$ with M = V and Ni. The densities of states calculated with the Extended Hückel approach (Figure 3) exhibit some significant differences as well as common features. In both cases, a peak occurs between ca. −12 and −15 eV, which consists mainly of the *5p* states of antimony. (The *5s* states are located below the energy window shown.) The contributions of each of Hf, V, and Ni to this peak point to covalent character of the metal−Sb bonds. The different chemistry of the M atoms vanadium and nickel is reflected in some differences in the densities of states: whereas the *3d* states of nickel are located in a sharp peak at −10 eV (well below the Fermi level of −8.56 eV), the vanadium states are extended broadly from ca. −10 eV up to well above the Fermi level of −8.09 eV). In the latter case, the M states occur in basically the same energy area as the Hf states. It is concluded that the *d* orbitals of Ni are more or less completely filled, whereas the V and Hf *d* states are partly occupied. This occurs with a significant number of states filled at the Fermi level for both $Hf_{10}MSb_5$ phases, which is larger in the case of M = V.

For an evaluation of the bonding situations, the semiempirical Hf−Hf, Hf−M, and Hf−Sb COOP curves, summed over all interactions in the unit cell, are shown in Figure 4. Averaged over the first Brillouin zone, almost no antibonding states are filled. Almost no Hf−Sb states occur at the

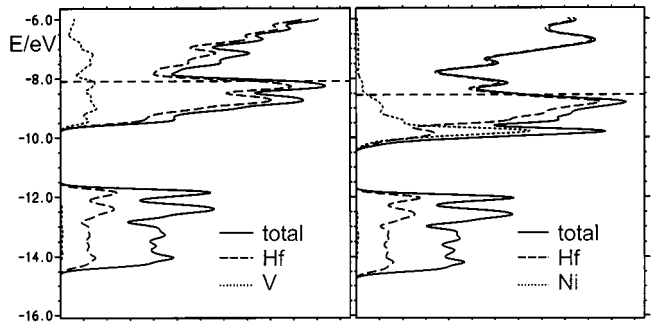

Figure 3. Calculated densities of states for $Hf_{10}MSb_5$ (EH approximation); left: M = V; right: M = Ni; horizontal lines: Fermi levels; solid line: total DOS; dashes: Hf contribution; dots: M contribution

Fermi level, which is dominated by bonding Hf−Hf interactions. Increasing the number of valence electrons would occur with more filled bonding Hf−Hf states, but with some filled antibonding Hf−M states in $Hf_{10}NiSb_5$. The Hf−V interactions are still bonding at the Fermi level (140 valence electrons), but become antibonding in character above −7.73 eV (ca. 151 valence electrons).

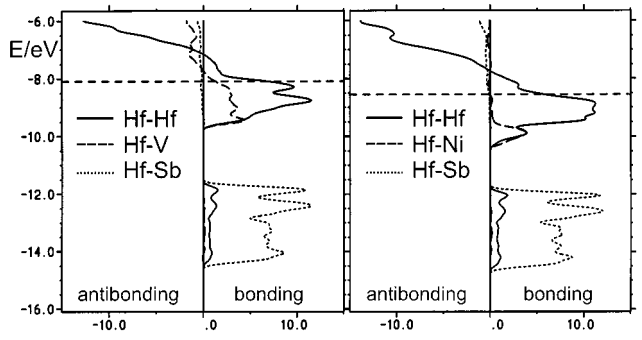

Figure 4. Selected summed COOP curves for $Hf_{10}MSb_5$; left: M = V; right: M = Ni; horizontal lines: Fermi levels; solid line: Hf−Hf interactions; dashed: Hf−M; dots: Hf−Sb; right parts of the diagrams: bonding interactions (+); left: antibonding (−)

After having considered some general features of the electronic structures, we focus now on the different structure models. In contrast to the model **III**, no homoatomic contacts occur in the (M,Sb) chains of models **I** and **II**. In model **I**, the M−Sb bonds of ca. 280 pm have net positive overlap populations although some antibonding states are filled in both cases (Figure 5). As a consequence of the filled *d* orbitals of nickel, antibonding Ni−Sb states occur above −10.5 eV, whereas fewer antibonding V−Sb states are filled. In addition to the differences in the antibonding states, the differences in the Mulliken overlap populations (*OP*) per bond (Ni−Sb: *OP* = 0.086; V−Sb: *OP* = 0.240) are also due to size effects (besides the dependence on the basis functions used): because of the smaller radius of nickel, a smaller overlap between the Ni and Sb orbitals is expected, which reflects itself in a smaller Pauling bond order *PBO* with $d(PBO) = d(1) - 60$ pm log *PBO*[8] [*PBO*(Ni−Sb): 0.38; *PBO*(V−Sb) = 0.48]. Since the differences in the (M,Sb) chains of models **I** and **II** arise solely from through-bond coupling between the chains, the interchain distance of 780 pm means that they are negligible. In model **III**, these bonds are replaced by homoatomic, namely M−M and Sb−Sb, interactions. They have definite bonding character in the case of $Hf_{10}VSb_5$ (V−V: *OP* = 0.24; Sb−Sb = 0.33), whereas the Ni−Ni interactions in $Hf_{10}NiSb_5$ are basically nonbonding (*OP* = 0.02), again because of the filled *d* orbitals. On the other hand, the Sb−Sb overlap populations in $Hf_{10}NiSb_5$ are of the same scale as in $Hf_{10}VSb_5$ (0.34 vs. 0.33). Comparable linear Sb−Sb chains were discussed recently:[9,10] in the structures of $(Zr,V)_{13}Sb_{10}$ and $(Zr,V)_{11}Sb_8$, the calculations revealed 1-electron 2-center *sigma* Sb−Sb bonds, which is in agreement with the values of the overlap populations of ca. 0.33 electrons per bond.

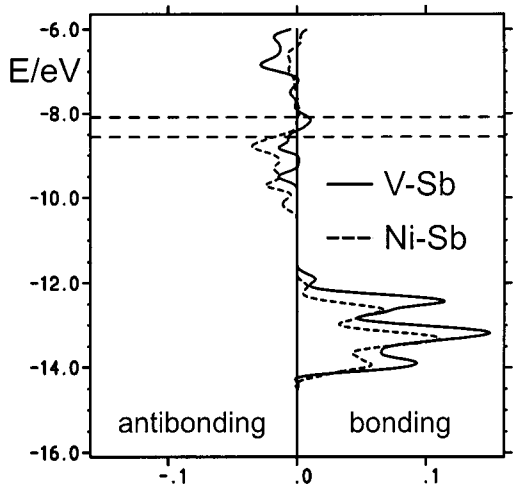

Figure 5. Averaged M−Sb COOP curves for $Hf_{10}MSb_5$; horizontal lines: Fermi levels; solid line: $Hf_{10}VSb_5$; dashed: $Hf_{10}NiSb_5$; right parts of the diagrams: bonding interactions (+); left: antibonding (−)

Based on the different Coulomb interactions one might expect that two M−Sb bonds are energetically favored relative to one M−M and one Sb−Sb bond. In the case of $Hf_{10}M_\delta Sb_{6-\delta}$, however, both M and Sb are somewhat negatively charged because of the more electropositive nature of hafnium, the major component of this phase. For example, the Pauling electronegativity values are 1.3 for hafnium, 1.6 for vanadium, 1.8 for nickel, and 1.9 for antimony. Correspondingly, the semiempirical Mulliken charges are −0.12 for vanadium and −0.49 for the Sb2 atom (Sb1: −0.67) in $Hf_{10}VSb_5$ (model **I**), and ≈0.00 for nickel and −0.43 for the Sb2 atom (Sb1: −0.49) in $Hf_{10}NiSb_5$ (model **I**). The metalloid antimony is obviously the most negatively charged atom, which renders reasonable the *antimonide* formulation for $Hf_{10}M_\delta Sb_{6-\delta}$. Furthermore, the Sb1 atom, being surrounded solely by Hf atoms, is more negatively charged than the Sb2 atom, which has two neighboring M atoms in model **I**. Both different kinds of Hf atoms show positive Mulliken charges, i.e. in the case of model **I** of $Hf_{10}VSb_5$ +0.17 for Hf1 and +0.38 for Hf2, and in the case of $Hf_{10}NiSb_5$ +0.06 for Hf1 and +0.29 for Hf2.

On the other hand, the charges of the M and Sb2 atoms obtained for model **III** differ significantly. The M atoms are

more and the Sb2 atoms less negatively charged in model **III** than in model **I** ($Hf_{10}VSb_5$: V −0.35 and Sb2 −0.07; $Hf_{10}NiSb_5$: Ni −0.22 and Sb +0.08). It is concluded that model **III** should exhibit a higher total energy because the Mulliken charges obtained are in direct contradiction to the trends expected based on electronegativity, especially for $Hf_{10}VSb_5$: the V atom exhibits a higher negative charge in model **III** than the Sb2 atom despite the lower electronegativity.

The entropy of an ordered structure generally differs from the disordered one by the configurational entropy. An estimation of the entropy of a completely disordered structure model $Hf_{10}MSb_5$, given by $\Delta S = -R\ \Sigma(X_i \ln X_i)$,[11] gives a value of 11.5 J/(molK). Since the free energy, ΔG, is determined by the equation $\Delta G = \Delta H - T\Delta S$, $T\Delta S$ is, besides the differences in the enthalpy, the factor which determines whether ordering occurs. According to our experiments, the minimum formation temperature of $Hf_{10}MSb_5$ is T = 1350°C, which corresponds to $T\Delta S = 0.2$ eV. Since this value is higher than the difference between the total energies of models **I** and **II** calculated with the LMTO method (0.02 eV in the case of $Hf_{10}NiSb_5$), one cannot expect complete (M,Sb) ordering from one chain to another.

The densities of states for the ordered structure model **I** of $Hf_{10}NiSb_5$, as obtained by the LMTO method, are shown in Figure 6. This shows that in contrast to the results of the Extended Hückel calculation, the peaks dominated by metal and antimony atoms do overlap. Furthermore, the overlap between the Hf and Ni states is more extensive than according to the EH calculations. The region around the Fermi level, however, is similar.

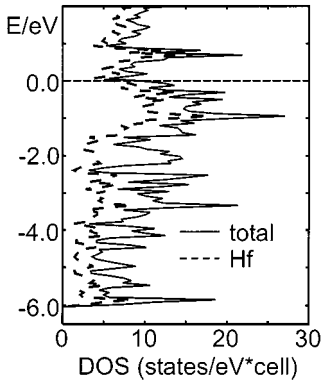

Figure 6. Calculated densities of states for $Hf_{10}NiSb_5$ (LMTO approach); DOS: Solid line: total DOS; dashes: Hf contribution

The significant densities of states at the Fermi level should occur with metallic properties, which is confirmed by several bands of $Hf_{10}NiSb_5$ crossing the Fermi level, as shown in Figure 7 which emphasizes the Ni centered bands with the fat band representation. The bands with a high Ni character occur about 2 eV below the Fermi level, which is reflected in a large Ni contribution to the densities of states in that energy area. Referring to the body-centered unit cell, two bands cross the Fermi level parallel to the c^* axis (symmetry lines ΓZ and XP), whereas no bands cross the Fermi level along the directions situated in the a^*,b^* plane, namely ΓX and PN. The latter is a consequence of the low dispersion of the Hf centered bands in the a,b plane, but does not imply one-dimensional metallic properties of all members of the $Hf_{10}M_{\delta}Sb_{6-\delta}$ series since the Fermi level depends on the number of valence electrons. The band structure of model **I** of $Hf_{10}VSb_5$ does not exhibit bands crossing the Fermi level along these symmetry lines, either, although that of $Hf_{10}FeSb_5$ does.

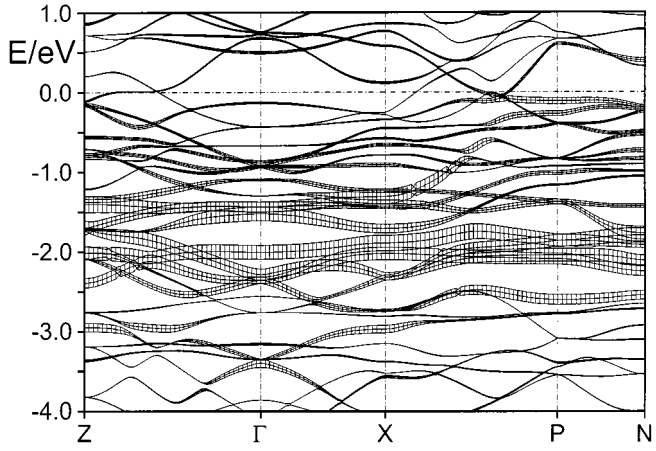

Figure 7. Band structure of $Hf_{10}NiSb_5$ (LMTO approach); fat bands projected on the Ni eigenvector contributions; symmetry points: Z = (−1/2, 1/2, 1/2); Γ = (0, 0, 0); X = (0, 0, 1/2); P = (1/4, 1/4, 1/4); N = (0, 1/2, 0) in units of the reciprocal primitive unit cell

Spin-polarized calculations within the local spin-density approximation were performed for the structure models containing the metal atoms Mn, Fe, Co, and Ni. Only in the case of $Hf_{10}FeSb_5$ was a magnetic ground state (0.6 μ_B) calculated. This occurred with a lowering of the total energy of just 4×10^{-5} eV relative to the non spin-polarized, and thus nonmagnetic, model calculation. The lower total energy is found to arise from a decrease in the number of states at the Fermi level, i.e. from 151 to 141 states/(eV × cell). The relatively small effects are a consequence of the small Fe content and the absence of any direct Fe−Fe interactions in $Hf_{10}FeSb_5$, while the difference between the energies of magnetic and (hypothetical) nonmagnetic α-Fe of 0.426 eV arises from a significant enhancement of Fe−Fe bonding.[12]

In order to check for a magnetic superstructure we carried out a spin-polarized self-consistent calculation of the tetragonal unit cell containing two (Fe,Sb) chains and thus two Fe atoms. The magnetic moments of the two Fe atoms were calculated to be +1.2 and −0.3 μ_B, respectively. Thus, the magnetic cell of $Hf_{10}FeSb_5$ in structure model **I** corresponds to the metric of the tetragonal unit cell in space group $P422$, with ferrimagnetic coupling between the Fe atoms of the two neighboring chains. However, different coupling of the magnetic moments of the Fe atoms resulted for the structure models **II** and **III**, namely ferromagnetic coupling with magnetic moments of 2.1 and 2.4 μ_B, respectively.

Physical Properties

The metal-rich composition, the presence of Hf−Hf contacts along all three directions, and the results of the electronic calculations discussed above strongly suggest metallic properties for all $Hf_{10}M_{\delta}Sb_{6-\delta}$ phases. The temperature dependence of the resistivity of a cold-pressed bar of the sample **II** (nominal composition $Hf_{10}CrSb_5$) is typical for a metallic sample (linearly increasing resistivity with increasing temperature), but the $\rho_{(10K)}/\rho_{(280K)}$ ratio of 0.94 is rather high. According to the Matthiesen rule $\rho(T) = \rho_i + \rho_L(T)$, the impurity contribution ρ_i to the measured resistivity $\rho(T)$ is basically independent of the temperature.[13] It is concluded that the contribution ρ_i is relatively large in this case, relative to the intrinsic lattice resistivity $\rho_L(T)$, thus leading to a small temperature dependence of the resistivity measured. This could be a consequence of either large grain boundaries or of an oxidation of the surface by oxygen, which we tried to minimize by working under an inert atmosphere in a glove-box as far as possible.

The metallic properties reflect themselves in the Pauli paramagnetism experimentally observed for the bulk samples of the initial compositions $Hf_{10}MSb_5$ with M = V, Co, and Ni (Figure 8). Aside from small Curie tails at low temperatures, the curves are basically temperature independent, indicating that no unpaired localized electrons are present in the samples investigated. On the other hand, the sample with the initial composition $Hf_{10}FeSb_5$ exhibits a slope typical of weak ferromagnetic or ferrimagnetic materials. This is in agreement with the results of the spin-polarized LMTO calculation, which yielded a magnetic moment only in the case of $Hf_{10}FeSb_5$.

Similar results were found experimentally for the antimonides Zr_5MSb_3 (Ti_5Ga_4 type): in the case of M = Fe ferromagnetic properties were observed, while Zr_5CoSb_3 and Zr_5NiSb_3 showed Pauli paramagnetism.[14]

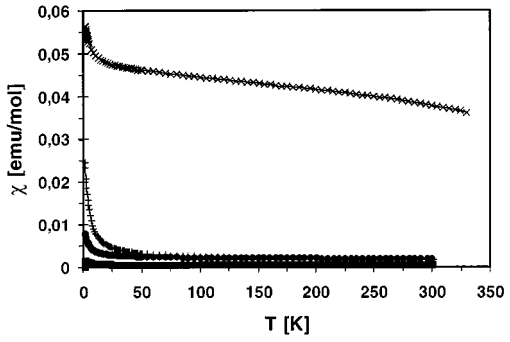

Figure 8. Temperature-dependence of the molar susceptibilities at 1 Tesla. ×: $Hf_{10}FeSb_5$; +: $Hf_{10}VSb_5$; filled circles: $Hf_{10}CoSb_5$; filled squares: $Hf_{10}NiSb_5$

To check for the ferromagnetic behavior, a field-dependent magnetization was measured at 5 Kelvin (Figure 9). Whilst the slope is familiar from ferromagnetic compounds, the hysteresis is almost zero, pointing to a very weak ferromagnetic material. The magnetic moment per Fe atom of 2 μ_B, as determined from an estimation of the saturation magnetization, suggests that the sample investigated consisted of different domains, i.e. a mixture of the different structure models, since the models **I**, **II** and **III** exhibit magnetic moments of 0.6, 2.1 and 2.4 μ_B, respectively (according to the LMTO calculations).

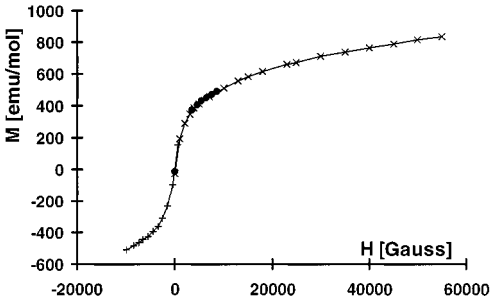

Figure 9. Field dependence of the magnetization *M* of $Hf_{10}FeSb_5$ at 5 Kelvin. +: 1. Series, *M* measured from 0 to 55000 Gauss; ×: 2. Series, field dropped rapidly from 55000 to 500 Gauss, then *M* measured from 500 Gauss to −10000 Gauss; filled circles: 3. Series, field increased rapidly to 0, then *M* measured from 0 to 8500 Gauss

Conclusions

The new antimonides $Hf_{10}M_{\delta}Sb_{6-\delta}$ (M = V, Cr, Mn, Fe, Co, Ni, Cu) were synthesized and subsequently characterized by single crystal structure studies, calculations of the electronic structures, and measurements of the magnetic and electrical properties of selected samples. The compounds $Hf_{10}M_{\delta}Sb_{6-\delta}$, exhibiting a phase range of at least $0.80(4) \leq \delta \leq 1.54(6)$, crystallize in the W_5Si_3 structure type. The X-ray experiments revealed no long-range ordering of the M/Sb atoms on the Si site. The calculations suggest that an ordering within a given (M,Sb) chain is likely to occur, but the correlation between the chains are too small for systematic ordering between the chains. The disordering can be explained by an increase of the configurational entropy, compared to the ordered structure model. The phases $Hf_{10}M_{\delta}Sb_{6-\delta}$ are metallic without localized magnetic moments, except for M = Fe, where weak ferromagnetic properties are detected experimentally, in agreement with theoretical calculations based on the spin-polarized LMTO method.

Experimental Section

Syntheses: In order to minimize the loss of antimony during the process of arc-melting, we first prepared $HfSb_2$ as the antimony source in a fused silica tube at 650°C, starting from the elements in the stoichiometric 1:2 ratio (Hf: STREM, powder, 99.6% (including up to 2.2% zirconium), Sb: MERCK, powder, 99.8%). The compounds $Hf_{10}MSb_5$ were synthesized by arc-melting of stoichiometric ratios of Hf, $HfSb_2$ and M on a water-cooled copper hearth under a flow of argon (3 L/min). With weight losses of typically between 1 and 4 weight-%, the yields can be optimized by adding a small excess of antimony. Attempts to synthesize $Hf_{10}MSb_5$ with different *3d* metals M (from vanadium to copper, all powder; V: ABCR, −45 micron, 99.7%; Cr: VENTRON, −50 mesh, 99.8%; Mn: VENTRON, −325 mesh, 99.9%; Fe: STREM, 99.999%; Co: ALFA, −50 mesh, 99.8%; Ni: VENTRON, −150 mesh, 99.9%; Cu:

Table 3. Selected reactions with Hf: (M + Sb) = 10: 6 (M = V, Cr, Mn, Fe, Co, Ni, Cu)

No.	M	M: Sb ratio	reaction conditions	main products
I	V	1: 5	arc-melting	$Hf_{10}V_{\delta}Sb_{6-\delta}$*
II	Cr	1: 5	arc-melting	$Hf_{10}Cr_{\delta}Sb_{6-\delta}$
III	Mn	1: 5	arc-melting	$Hf_{10}Mn_{\delta}Sb_{6-\delta}$
IV	Fe	1: 5	arc-melting	$Hf_{10}Fe_{\delta}Sb_{6-\delta}$
V	Co	1: 5	arc-melting	$Hf_{10}Co_{\delta}Sb_{6-\delta}$
VI	Ni	1: 5	arc-melting	$Hf_{10}Ni_{\delta}Sb_{6-\delta}$
VII	Cu	1: 5	arc-melting	$Hf_{10}Cu_{\delta}Sb_{6-\delta}$
VIII	V	1: 5	arc-melting, then annealing at 900 °C	$Hf_{10}V_{\delta}Sb_{6-\delta}$*
IX	Ni	1: 5	arc-melting,then annealing at 900 °C	$Hf_{10}Ni_{\delta}Sb_{6-\delta}$*
X	Mn	1: 5	annealing at 1350 °C	$Hf_{10}Mn_{\delta}Sb_{6-\delta}$*
XI	Fe	2: 4	arc-melting	$Hf_{10}Fe_{\delta}Sb_{6-\delta}$* + ?
XII	Fe	1.75: 4.25	arc-melting	$Hf_{10}Fe_{\delta}Sb_{6-\delta}$ + ?
XIII	Fe	1.5: 4.5	arc-melting	$Hf_{10}Fe_{\delta}Sb_{6-\delta}$
XIV	Fe	1.25: 4.75	arc-melting	$Hf_{10}Fe_{\delta}Sb_{6-\delta}$
XV	Fe	0.75: 5.25	arc-melting	$Hf_{10}Fe_{\delta}Sb_{6-\delta}$
XVI	Fe	0.5: 5.5	arc-melting	$Hf_{10}Fe_{\delta}Sb_{6-\delta}$ + Hf_5Sb_3
XVII	Fe	0.25: 5.75	arc-melting	$Hf_{10}Fe_{\delta}Sb_{6-\delta}$ + Hf_5Sb_3

*: Single crystal structure study.

Table 4. Lattice parameters of $Hf_{10}MSb_5$

No.	M	*a*/pm	*c*/pm	*V*/(10^6pm^3)
I	V	1095.54(9)	558.08(9)	669.8
II	Cr	1094.06(5)	556.54(1)	666.2
III	Mn	1093.70(4)	556.52(6)	665.7
IV	Fe	1091.5(1)	555.22(8)	661.5
V	Co	1091.3(1)	553.7(1)	659.4
VI	Ni	1092.6(1)	552.7(1)	659.8
VII	Cu	1093.74(5)	554.01(6)	662.7

VENTRON, 99.9%) were successful in all cases, according to the powder diagrams of all reaction products and EDX investigations on selected samples ($Hf_{10}VSb_5$ and $Hf_{10}NiSb_5$, numbers **I** and **VI** in Table 3). An analogous reaction using titanium (Ti: ALFA, −100 mesh, 99.4%) instead of hafnium resulted in the formation of Ti_5NiSb_3[15] as the main product. A reaction using titanium as the *3d* metal did not yield the hypothetically isostructural "$Hf_{10}TiSb_5$", but resulted in the formation of the hitherto unknown compound $(Hf,Ti)_7Sb_4$[16] as the main product. Table 4 lists the lattice parameters obtained from the ground samples with the Guinier technique (Cu-K_{α}, using silicon as internal standard).

A single crystal of the sample **I** was investigated on an IPDS diffractometer (STOE). Parts of **I** and **VI** were annealed over a period of three weeks at 900 °C in tantalum tubes, placed in fused silica tubes sealed under vacuum. No differences were observed between the powder diagrams obtained before and after the annealing procedure. Nevertheless, the annealed samples of the initial compositions $Hf_{10}VSb_5$ (**VIII**) and $Hf_{10}NiSb_5$ (**IX**) were investigated also

Table 5a. Crystallographic data for $Hf_{10}V_{0.80(4)}Sb_{5.20}$ and $Hf_{10}V_{0.88(4)}Sb_{5.12}$

Empirical formula	$Hf_{10}V_{0.80(4)}Sb_{5.20}$	$Hf_{10}V_{0.88(4)}Sb_{5.12}$
Synthesis	arc-melting	arc-melting + annealing
Molar mass	2458.8 g/mol	2453.1 g/mol
T. of data collection	295 K	295 K
Crystal size /mm^3	0.04 × 0.02 × 0.01	0.03 × 0.02 × 0.01
Space group	*I4/mcm*	*I4/mcm*
a/pm	1097.1(2)	1097.1(2)
c/pm	558.17(9)	560.4(1)
V/(10^6pm^3)	671.8(2)	674.5(2)
No. of f. u.; F(000)	2; 1003	2; 1002
Calculated density	12.15 g/cm^3	12.08 g/cm^3
Absorption coefficient	87.58 mm^{-1}	22.87 mm^{-1}
Range of 2θ	3° − 60°	3° − 60°
No. of independent reflections	298 (R_{int} = 0.083)	297 (R_{int} = 0.065)
No. of observed reflections (I>2σ(I))	232	214
No. of parameters	17	17
R(F), $R_w(F^2)$, GOF	0.028, 0.065, 1.05	0.023, 0.040, 0.97
Extinction coefficient	0.00009(5)	0.00035(4)
Absorption correction	numerical	numerical
Min., max. transmission	0.10, 0.67	0.09,0.37
Max., min. peak in final diff. map	2.42 e$^-$/(10^6pm^3), −2.94 e$^-$/(10^6pm^3)	2.50 e$^-$/(10^6pm^3), −2.94 e$^-$/(10^6pm^3)

Table 5b. Crystallographic data for $Hf_{10}Mn_{1.1(1)}Sb_{4.88}$, $Hf_{10}Fe_{1.54(6)}Sb_{4.46}$ and $Hf_{10}Ni_{1.18(6)}Sb_{4.82}$

Empirical formula	$Hf_{10}Mn_{1.16(10)}Sb_{4.84}$	$Hf_{10}Fe_{1.54(6)}Sb_{4.46}$	$Hf_{10}Ni_{1.18(6)}Sb_{4.82}$
Synthesis	annealing	arc-melting	arc-melting + annealing
Molar mass	2437.9 g/mol	2410.0 g/mol	2441.0 g/mol
T. of data collection	295 K	295 K	295 K
Crystal size /mm^3	0.02 × 0.02 × 0.01	0.03 × 0.02 × 0.02	0.01 × 0.01 × 0.005
Space group	*I4/mcm*	*I4/mcm*	*I4/mcm*
a/pm	1094.0(2)	1085.9(2)	1097.1(2)
c/pm	555.2(1)	554.0(1)	558.9(1)
V/(10^6 pm^3)	664.5(3)	653.2(2)	672.7(2)
No. of f. u.; *F*(000)	2; 996	2; 988	2; 999
Calculated density	12.19 g/cm^3	12.27 g/cm^3	12.05 g/cm^3
Absorption coefficient	88.35 mm^{-1}	89.68 mm^{-1}	87.80 mm^{-1}
Range of 2θ	3° − 60°	3° − 60°	3° − 60°
No. of independent reflections	292 (R_{int} = 0.196)	288 (R_{int} = 0.092)	298 (R_{int} = 0.088)
No. of observed reflections (*I*>2σ(*I*))	144	213	223
No. of parameters	17	17	17
R(*F*), $R_w(F^2)$, GOF	0.041, 0.082, 0.89	0.028, 0.058, 0.99	0.031, 0.069, 0.93
Extinction coefficient	0.00000(4)	0.00001(4)	0.00052(8)
Absorption correction	numerical	numerical	numerical
Min., max. transmission	0.12, 0.23	0.09, 0.37	0.14, 0.59
Max., min. peak in final diff. map	3.46 e$^-$/(10^6pm^3), −4.53 e$^-$/(10^6pm^3)	2.27 e$^-$/(10^6pm^3), −2.64 e$^-$/(10^6pm^3)	4.04 e$^-$/(10^6pm^3), −3.14 e$^-$/(10^6pm^3)

by single crystal structure analyses. Reactions starting from $HfSb_2$, Hf, and different M atoms, carried out in sealed tantalum tubes without previous arc-melting, did not result in the formation of the $Hf_{10}M_{\delta}Sb_{6-\delta}$ phases after annealing for six days at temperatures of 1300°C. At a reaction temperature of 1350°C, $Hf_{10}Mn_{\delta}Sb_{6-\delta}$ formed, and a single crystal study was also performed using a small crystal of this sample (**X**).

A study of the phase range was carried out in the Hf−Fe−Sb system by arc-melting different mixtures, corresponding to the starting compositions of "$Hf_{10}Fe_{\delta}Sb_{6-\delta}$" with δ = 2, 1.75, 1.5, 1.25, 0.75, 0.5 and 0.25. At δ = 2 and 1.75, the phase $Hf_{10}Fe_{\delta}Sb_{6-\delta}$ formed together with other unidentified products, and at δ = 0.5 and 0.25, the hitherto unknown binary antimonide Hf_5Sb_3[17] was detected, as well as $Hf_{10}Fe_{\delta}Sb_{6-\delta}$. It is concluded that the phase range is within $0.5 < \delta < 1.75$. Correspondingly, a single crystal study of the sample with δ = 2 (**XI**) yielded the formula $Hf_{10}Fe_{1.54(6)}Sb_{4.46}$, and thus δ = 1.54(6).

Single-Crystal Studies: All five data sets were collected with an IPDS diffractometer. The data were corrected for Lorentz and polarization effects. No superstructure reflections were observed in any of these data sets. The structure solutions and refinements were performed using SHELXS86 and SHELXL97.[18] The systematic extinction of $l = 2n + 1$ for all *0kl* reflections (in addition to the integral extinctions, namely $h + k + l = 2n + 1$) restricted the possible space groups to *I*4/*mcm* (W_5Si_3), *I*4*cm* and $I\bar{4}c2$. The *4a* position of *I*4/*mcm*, which is occupied by a mixture of M and Sb atoms, has the multitude of four in all three space groups. To check for ordering on this site, all five structure models were refined in the space group *I*4*22*, which allows alternating M and Sb atoms within the (M,Sb) chains by splitting the *4a* site of *I*4/*mcm* into *2a* and *2b*. No ordering was observed. Final refinements in the space group *I*4/*mcm* yielded, in all cases, different ratios of the M and Sb atoms in this chain, which were refined under the restriction of $f_M + f_{Sb} = 1$, i.e. 100% occupancy in the sum of the occupancies of the M and Sb atoms. The results are summarized in the Tables 2, 5a and 5b.[19]

Calculations of Electronic Structures: Semiempirical band-structure calculations were performed using the Extended Hückel approximation.[20−22] The metal parameters were optimized by alternating charge iterations until convergence using constant Sb parameters (Table 6). The tetragonal cell (80 *k* points) was chosen for all calculations for consistency, because not all models considered exhibited the body-centered symmetry (see main text).

More sophisticated electronic calculations were carried out with the self-consistent TB-LMTO-ASA program within the local-density approximation.[23−25] The integration in *k* space was performed by the tetrahedron method[26] on a grid of 1331 irreducible *k* points. The *5f* orbitals of hafnium and the *4f* orbitals of antimony were included by using a downfolding technique. The symmetry points of the band structure were chosen according to Bradley and Cracknell.[27]

Table 6. Parameters used for EH calculations

Orbital	H_{ii}/eV	ζ_1	c_1	ζ_2	c_2
Hf, 6s	−7.79[a]/−8.14[b]	2.21			
Hf, 6p	−4.27[a]/−4.57[b]	2.17			
Hf, 5d	−7.62[a]/−8.08[b]	4.36	0.6967	1.709	0.5322
V, 4s	−7.49	1.30			
V, 4p	−4.00	1.30			
V, 3d	−7.95	4.75	0.4755	1.70	0.5798
Ni, 4s	−7.63	1.925			
Ni, 4p	−3.58	1.925			
Ni, 3d	−9.55	5.75	0.5862	2.20	0.5845
Sb, 5s	−18.80	2.32			
Sb, 5p	−11.70	2.00			

[a] Values for the calculation on $Hf_{10}VSb_5$. − [b] Values for the calculation on $Hf_{10}NiSb_5$.

Transport Properties: Temperature dependent resistivity measurements were performed on a cold-pressed bar with the nominal composition $Hf_{10}CrSb_5$. The pellet was contacted at four points, which enables a measurement independent of the resistivities of the contacts.

Magnetic Properties: Magnetic data were obtained for the bulk samples of $Hf_{10}M_1Sb_5$ with M = Fe, V, Co, and Ni. Temperature-dependent measurements were made at 1 Tesla in the temperature range of 1.8−300 K on a Quantum Design MPMS SQUID magnetometer. The data were corrected for the diamagnetic atom cores.

Acknowledgments

The experimental work was carried out at the Department of Chemistry, University of Marburg. Financial support from the "Deutsche Forschungsgemeinschaft", the "Fonds der Chemischen Industrie" and the "Bundesministerium für Bildung, Wissenschaft, Forschung und Technologie" is gratefully acknowledged. Insightful discussions with Professor Dr. B. Harbrecht are appreciated.

[1] P. Villars, L. D. Calvert, *Pearson's Handbook of Crystallographic Data for Intermetallic Phases*, 2nd Edition, ASM, Materials Park, OH 1996.
[2] I. Schewe-Miller, P. Böttcher, *J. Alloys Compd.* **1992**, *183*, 98−108.
[3] R. Berger, *Acta Chem. Scand.* **1977**, *31A*, 223−226.
[4] Y.-U. Kwon, S. C. Sevov, J. D. Corbett, *Chem. Mater.* **1990**, *2*, 550−556.
[5] H. Kleinke, H. F. Franzen, *J. Solid State Chem.* **1998**, *136*, 221−226.
[6] L. Zeng, H. F. Franzen, *J. Alloys Compd.* **1998**, *270*, 119−122.
[7] H. Kleinke, *J. Alloys Compd.* **1998**, *270*, 136−141.
[8] L. Pauling, *The Nature of the Chemical Bond*, Cornell University Press, Ithaca, NY, 3rd ed., 1948.
[9] H. Kleinke, *Chem. Commun.* **1998**, 2219−2220.
[10] H. Kleinke, *J. Mater. Chem.* **1999**, *9*, 2703−2708.
[11] H. F. Franzen, J. A. Merrick, *J. Solid State Chem.* **1980**, *33*, 371−374.
[12] G. A. Landrum, R. Dronskowski, *Angew. Chem. Int. Ed.* **1999**, *38*, 1389−1393.
[13] C. Kittel, *Introduction to the Solid State Physics*, New York, Wiley, 7th ed., **1996**.
[14] E. Garcia, H. C. Ku, R. N. Shelton, J. D. Corbett, *Solid State Comm.* **1988**, *65*, 757−760.
[15] W. Rieger, E. Parthé, *Acta Crystallogr.* **1968**, *24B*, 456−458.
[16] H. Kleinke, *Inorg. Chem.* **1999**, *38*, 2931−2935.
[17] H. Kleinke, C. Felser, *J. Alloys Compd.* **1999**, *291*, 73−79.
[18] G. M. Sheldrick, *SHELXS86*, University of Göttingen, **1986**; *ibid.*, *SHELXL93*, **1993**.
[19] Further details of the crystal-structure investigations may be obtained from the Fachinformationszentrum Karlsruhe, D-76344 Eggenstein-Leopoldshafen, Germany, on quoting the depository numbers CSD-410803 − CSD-410807.
[20] R. Hoffmann, *J. Chem. Phys.* **1963**, *39*, 1397−1412.
[21] M.-H. Whangbo, R. Hoffmann, *J. Am. Chem. Soc.* **1978**, *100*, 6093−6098.
[22] Program EHMACC, adapted for use on a PC by M. Köckerling, Gesamthochschule Duisburg, 1997.
[23] L. Hedin, B. I. Lundqvist, *J. Phys.* **1971**, *C4*, 2064−2083.
[24] O. K. Andersen, *Phys. Rev.* **1975**, *B12*, 3060−3083.
[25] H. L. Skriver, *The LMTO Method*, Springer, Berlin, **1984**.
[26] O. Jepsen, O. K. Andersen, *Solid State Commun.* **1971**, *9*, 1763−1767.
[27] C. J. Bradley, A. P. Cracknell, *The Mathematical Theory of Symmetry in Solids*, Clarendon Press, Oxford, **1972**.

Received June 10, 1999
[I99220]